

ScienceDirect

Procedia MANUFACTURING

www.elsevier.com/locate/procedia

Procedia Manufacturing 00 (2019) 000-000

48th SME North American Manufacturing Research Conference, NAMRC 48, Ohio, USA

Thin wall deposition of IN625 using directed energy deposition

Myong Joon Kim, Christopher Saldana*

George W. Woodruff School of Mechanical Engineering, Georgia Institute of Technology, 801 Ferst Drive, Atlanta, Georgia 30332

* Corresponding author. E-mail address: christopher.saldana@me.gatech.edu

Abstract

Laser powder-blown directed energy deposition (DED) is widely used for small feature deposition ability and geometrical accuracy. The effects of process parameters, control, and toolpath strategies on geometry of the final product and mechanical properties have been investigated in many different parent geometries, however, deposition on an existing thin feature that has less width than the diameter of the laser spot size has yet to be addressed and is critical for various component repair applications. This study quantifies controllable factors contributing to optical characterization, geometry, characteristics of internal porosity, and microstructure of the deposit in the deposition processes of Inconel 625 by the laser powder-blown DED method. A full-factorial experimental plan was arranged with variations in laser power (175W to 275W) and mass flowrate (2g/min to 20g/min) on thin (0.5mm) and thick (3.0mm) substrate deposition. These results are useful for deriving an optimal workpiece quality through adjustment of controllable process parameters.

© 2019 The Authors. Published by Elsevier B.V.

This is an open access article under the CC BY-NC-ND license (http://creativecommons.org/licenses/by-nc-nd/3.0/)
Peer-review under responsibility of the Scientific Committee of NAMRI/SME.

Keywords: hybrid manufacturing, digitization, adaptive repair, remanufacturing

1. Introduction

Additive manufacturing (AM) has been recognized as a viable method to create or repair intricate parts or features. AM parts are widening its horizon in being used in automotive, aerospace, and marine industry for being time- and costefficient for highly complex or valued parts which cannot be newly manufactured or remanufactured otherwise [1, 2]. Due to the great capabilities and demand from the industry, quality, consistency, reliability, and finishing of AM have been utmost importance in research. Turbine blades, vanes, blisks, and casing to name a few that are highly expensive parts which are usually remanufactured to extend the serviceable life [3]. Benefits of DED is that this not only inherits great degree of freedom in manipulating process parameters to optimize final geometry, but also maintains consistency in repeated production with selected parameters compared to manual welding or wire DED. Although the weld geometry can be

adaptively machined using digitization methods in hybrid manufacturing cell, accurately achieving final geometry with controlled parameters is desired [4].

Laser powder-blown directed energy deposition (DED) is a rapid manufacturing technology that deposits metal by using focused laser as a heat source to partially melt the substrate and blown metallic powder to fabricate 3D object. DED has many potential applications, but due to the low production rate compared to conventional manufacturing methods, it is especially suitable for replacing manual welding in repair process for improved consistency and flexibility to be implemented in various part geometry. DED has advantages over laser powder-bed fusion in that it has higher deposition rate, less limited component size, higher powder efficiency, and ability to repair on existing parts.

This study focuses on single bead deposit on a thin substrate so to establish relationships between process parameters and deposition results. There are numerous studies on laser DED, but none addressed the effect of process parameters on depositing material on an existing thin substrate that has smaller width than the laser diameter. Power, mass flowrate, and width of substrate compared to laser diameter were deposition parameters that were varied which contribute to energy density and powder deposition density [5]. Surface discoloration, geometrical characteristics, porosity/void analysis, and microstructure of the deposit and of fusion boundary were considered dependent variables. Microstructural as characterization has been studied and related with varying process parameters which directly affect thermal activity and energy input of the laser [6-9]. Ref. [6] constructed an outcome linked to process parameters for DED of Inconel 625 that identifies solidification morphology and microstructural scale. Ref. [7] discovered that dendrites and elongated grains form in the direction of the highest temperature gradient, whereas Ref. [8] concluded that the columnar dendrites grew in the direction of laser scan. Ref. [9] showed solidification of oriented dendrites is locally perpendicular to the travel direction, and aligned at 45 degrees to the substrate. Microstructure is often tied with mechanical properties such as ultimate tensile strength, ductility, and hardness. [7, 10, 11] The Vickers hardness in AM IN625 is higher than conventionally-processed metal due to the presence of secondary phases and fine dendritic structures within grains. The effect of process parameters on porosity and defects were studied and prediction models were generated. [12-14] Geometric characterization was studied with height, width, aspect ratio, and diffusion. Interfacial phenomena and characteristics between deposit and substrate of IN625 as well as track geometry as a result of process parameters in different materials have been extensively studied in AM for decades. [15-25] Ref. [15] characterized continuity, consistency, width, height, height, surface roughness, and microstructure of single bead deposit on substrate. Ref. [19] established a semi-empirical equation to predict geometric characteristic of deposited bead. Ref. [21] demonstrated that using infrared temperature signal emitted from melt pool, better dimensional accuracy can be achieved and hot-cracking can be avoided when nickel-based super alloy is deposited as a thin wall. Ref [25] compared geometry, hardness, and dilution of single track deposit on a flat substrate against that on edge. Ref. [26, 27] used closed-loop control and Ref. [28] used real-time control of DED to provide better control of final bead geometry.

In this paper, in order to curtail efforts in post-processing by controlling final geometry and to produce high quality parts without internal defects, suitable process parameter combinations are analyzed and determined by experimental methods. Geometric characteristics were measured and confirmed with 2D X-ray scans. Volumetric percent porosity was determined with 3D reconstructed CT scan of single track deposit on Volume Graphics software. Microstructural characteristics such as grain structure and grain size in the surface area, boundary between the deposit and the substrate, and inside of the deposit were analyzed after etching the transverse cross-sectional area of the deposit and inspecting under digital microscope. Hardness in the same region where microstructure were inspected was measured to relate mechanical property to microstructure. Visual inspection on the

surface of the deposit was conducted to check discoloration of the surface if there is any oxidation on the surface.

INCONEL 625 is used as powder and substrate in this study since it is widely used in aerospace repair applications for its excellent weldability and availability. The material also retains high yield strength, creep strength, fatigue strength, and oxidation/corrosion resistance in aggressive environments that makes it a great candidate. [8]

2. Material and methods

2.1 Materials and DED processing

INCONEL® nickel-chromium alloy 625 (IN625) was vacuum induction melted followed by inert gas atomization with argon to produce IN625 powder (Praxair). The powder was sieved with -125 μ m/+45 μ m with apparent density of 0.1554lbs/in³ and melting temperature between 2300F to 2437F. The weight percent chemical composition of IN625 is presented in Table 1.

The powder was carried from the powder hopper by argon and fed around the laser coaxially. Powder mass flow rate was controlled by the metering disk ranging from 2g to 150g/min depending on the type of powder, application and the groove size of the metering disk with the accuracy of +/-1%. The powder was used to fabricate parts using a Mazak VC-500 AM machine, which has 5-axis subtractive and additive capability with XYZ on the tool head and B/C on the table control. The manufacturing cell fitted with Hybrid Manufacturing Technology additive head and a 1kw continuous wave IPG Photonics YLR fiber laser. The laser has output stability of +/-2.0% and has a focal distance of 100mm from the end of the lens with the laser spot size of 1.0mm.

2.2 Test process parameters

Tracks were deposited on annealed IN625 sheet metal that has density of 0.31 lbs/in³, hardness of Rockwell B95, and thermal conductivity of 70 Btu/hr in/ft² at 70F. Substrate had two different thickness (W) 0.5mm and 3.0mm with five different laser power (P) from 175W to 275W and ten different mass flow rate (F) ranging from 2g/min to 20g/min. Traverse speed, carrier gas flow, shielding gas flow, and nozzle gas flow were controlled. Carrier gas flowrate and shielding gas flowrate

Table 1 Limiting chemical composition (%) of IN625

Nickel	58.0 min.
Chromium	20.0-23.0
Iron	5.0 max.
Molybdenum	8.0-10.0
Niobium (plus Tantalum)	3.15-4.15
Carbon	
Manganese	0.50 max.
Silicon	0.50 max.
PhosphorusSulfur	0.015 max.
Sulfur	0.015 max.
Aluminum	0.40 max.
Titanium	
Cobalt ^a	1.0 max.

were fixed at 6L to provide most consistent carrier flow that maximizes the powder flow supply efficiency within 1.0mm laser spot. The increase in powder supply efficiency was shown to result less porosity and penetration rate for better welding quality [29]. The process parameters are outlined in Table 2. Single track deposits were carried out on a thick plate to generalize the correlation between specific energy and powder density as well as the correlation between powder density and single-track height. Combinations of laser power, powder mass flowrate, and thickness of substrate gave 100 single track samples which were used to characterize the trend of the outcome from various sets of parameters.

Table 2 Process parameters

Laser power (Watts)	175, 200, 225, 250, 275
Powder mass flowrate (g/min)	2~20; increment of 2
Thickness of substrate (mm)	0.5, 3
Laser spot diameter (mm)	1.0
Focal distance (mm)	5.5
Feed rate (mm/min)	200
Carrier gas flowrate (L/min)	6
Shielding gas flowrate (L/min)	6
Nozzle gas flowrate (L/min)	2
Length of the track (mm)	12

2.3 Observation method

First, any discoloration on the surface of the track was inspected and pictures of top and side of all samples were taken. After visual inspection, samples were electrical discharge machined (EDM) for non-destructive analysis using CT with an isotropic 8µm-voxel resolution. 15 selected samples (three density settings 30, 50, 70, and five power settings 175W, 200W, 225W, 250W, 275W) were analyzed with CT where deposit qualities represented all extremities of samples. Single track samples were cut with small portion of substrate left on the deposits that had discoloration from the original color which indicated major HAZ. The direction of deposition of single track samples were aligned with Z-axis of CT scanner to minimize the length of penetration that X-ray had to go through for maximum contrast between air/void and material. The surface of the CT scans were first determined creating a threshold between two distinctive peaks (air and material). The threshold was then used to analyze porosity/void within each deposit. Star artifacts created from CT scans were removed in post-processing of the data. The high density of the material property caused x-ray scattering and caused beam hardening effect on the sharp corners. To increase the signal-to-noise ratio between the sample and the air and narrow the x-ray spectrum, a 0.5mm copper plate was placed in the source. The voltage and current were operated at 100kV and 80µA, respectively, to acquire 750 projections over 1 hour. Volume Graphics was utilized to reconstruct the internal geometry of the samples. A range of sizes of porosity was analyzed and performed using VGSTUDIO Max 3.1 made by Volume Graphics.

Following non-destructive analysis, the samples were cured in epoxy for 24 hours, polished, and etched to characterize microstructure at different locations of the deposit. Regions of interest were surface boundary, core of deposit, and interfacial boundary between parent material and deposit. The samples were evaluated under Leica DVM6 digital microscopy which can provide up to 2350X magnification at 425nm resolution.

3. Results

3.1 Optical characterization

For thin substrate deposition, the surface discoloration of single track deposits were analyzed by its top surface color. Shiny chrome color was shown in low range of mass flowrate (2 ~ 10g/min) and power (175W, 200W). Increasing mass flowrate turned the color to yellow, brown, and dark brown, and increasing laser power revealed more blue color on the surface. On the other hand, thick substrate deposition did not show any brown and blue discoloration until mass flowrate was equal to or greater than 16g/min and laser power between 200W and 275W. All other single tracks had shiny chrome color on the thick plate. Progressive change in surface discoloration of thin substrate deposition is shown in Fig2 at a fixed mass flowrate of 10g/min, and varying laser power.

Laser power was limited to 275W for thin plate deposition due to the substantial melting of the substrate as can be seen in Fig.1. With increase in mass flowrate with same power setting, height and width increased. Increasing laser power resulted more oxidation and blue/purple/brown coloring of the surface. No black or white color nor any scale, pores, cracks were present on the surface. The average depth of HAZ in the steady cladding region decreased with increase in mass flowrate when

Power	Top surface of single track at 10g/min
175W	
200W	
225W	Commission of the second
250W	
275W	— 1mm

Figure 1 Spectrum of discoloration on the top surface of single track deposit. Color changes from chrome to light blue to brown to dark brown and purple.

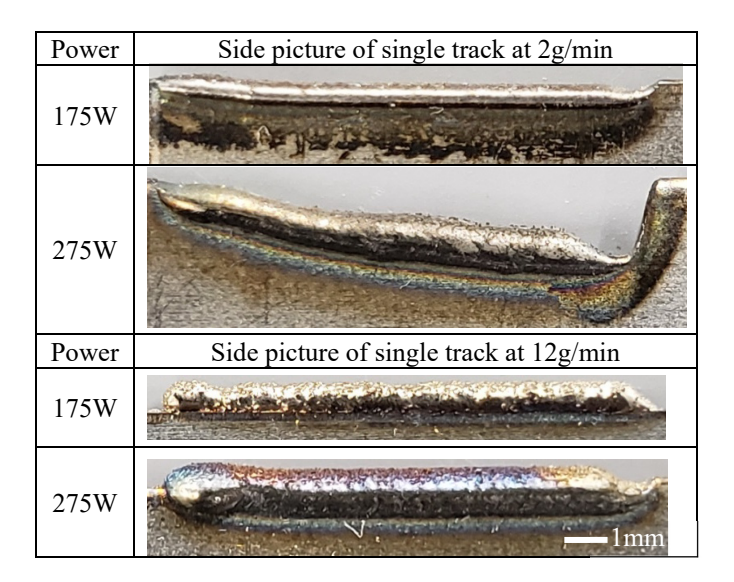


Figure 2 Representative discoloration of top surface of single track deposits at fixed mass flowrate of 2g/min and 10g/min and power of 175W and 275W.

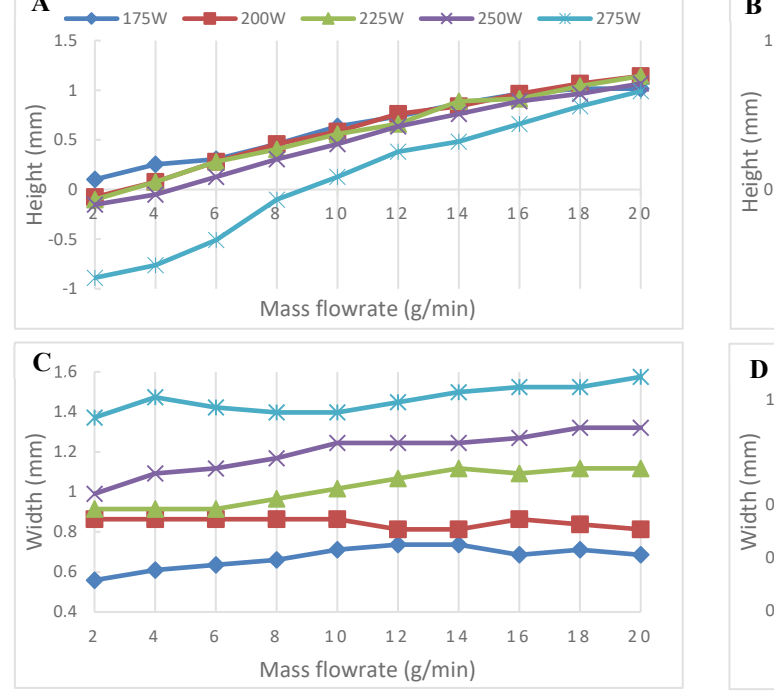
the laser power is between 175W and 225W, whereas it did not have a distinct trend in 250W and 275W conditions.

3.2 Geometric characterization

Single track deposits were geometrically measured in height and width with different process parameters and varying thickness of the substrate. For every track, five measurements were taken in the middle of the single track and averaged where it has steady cladding conditions. This region has an energy equilibrium between laser energy and heat dissipated by conduction through the melt pool and the base substrate material and convection through air for the span of short length [30] Height and width data at different laser power were plotted in Fig. 3 against mass flow.

The width of deposit on thin and thick substrate increased with increase in mass flowrate (2g/min to 20g/min) and laser power (175W to 275W). For the deposits on thin substrate, 1000% increase in mass flowrate increased the width as little as 6.25% at 200W, and as much as 33.3% at 250W. For each fixed power setting, increase in mass flowrate resulted increased width of the bead on average 21.69% with standard deviation of 11.45%. When there was 57% increase in laser power from 175W to 275W, width increased as little as 96.43%, and as much as 129.63%. For each fixed mass flowrate, increasing laser power resulted 110.43% increase in width on average with standard deviation of 17.30%. For the deposits on thick substrate, width increased as little as 13.51% and as much as 66.67%. On average, there was 33.78% average increase with respect to 1000% increase in mass flowrate with standard deviation of 20.67%. On the other hand, when laser power varied from 175W to 275W, width of the bead grew from 60% at 100g/min mass flowrate to 138.89% at 40g/min mass flowrate. The increase was 99.13% on average with standard deviation of 27.12%. Laser power has more dominant effect on the width of the single track deposit for both thin and thick substrate.

The height of deposit relative to the initial surface on a thin and thick substrate had increasing trend with respect to increase in mass flowrate, but laser power affected the height differently in thin substrate deposition. When the material was deposited on thin substrate, maximum height was reached at 200W and 225W at 20g/min of mass flowrate. On the other hand, the maximum height on thick substrate kept increasing as more



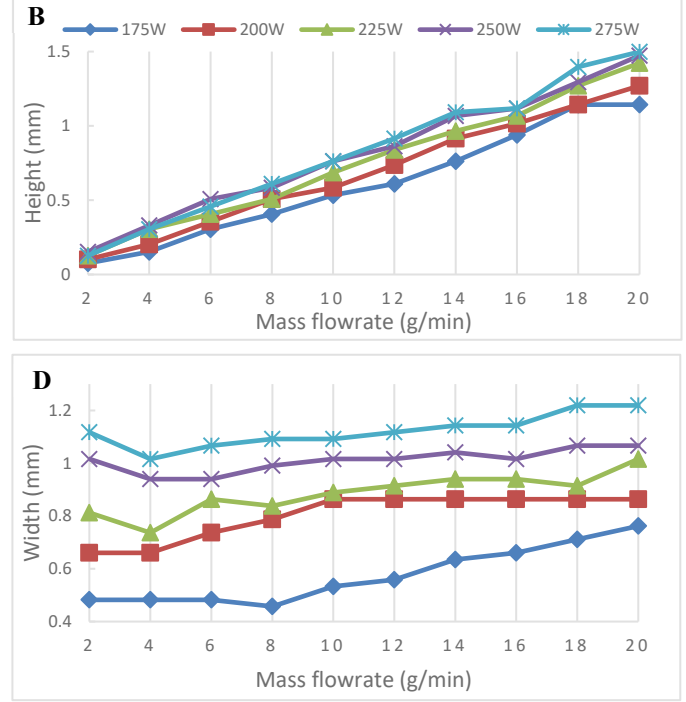


Figure 3 Geometric characteristics of single track deposit with varying mass flowrate and laser power. A) Height vs. mass flowrate of thin substrate deposition, B) height vs. mass flowrate of thick substrate deposition, C) width vs. mass flowrate of thin substrate deposition, D) width vs. mass flowrate of thick substrate deposition.

power was applied. This was because more power on the thin substrate could not be compensated with maximum powder provided and melted the substrate and decreased the final height. Negative height were seen in thin substrate deposition at high laser power and low mass flowrate. Power greater than 175W and mass flowrate of 2g/min all resulted in negative height. As power increased, it required more mass flowrate to compensate for melting the substrate. Single track deposit with negative height was mostly composed of the melted substrate therefore it was disregarded in the analysis.

3.3 Porosity analysis on CT scans

Volume Graphics was utilized to acquire porosity volume ratio (%), diameter, volume, and sphericity of pores of the deposit. A representative picture of deposit with pores (175W, 6g/min) that were color-mapped with corresponding diameter size is depicted in Fig. 4. Porosity volume ratio was plotted against three different mass flowrate and five laser power in Fig. 5A. As mass flowrate of the powder increased from 6g/min to 14g/min, there was an average of 0.48% increase in porosity to deposit volume ratio. However, the relationship between porosity volume ratios to laser power was inconclusive. While 175W had minimum percent porosity in all mass flowrates, 200W had maximum percent porosity for most cases, and other laser power had percent porosity values in between the two.

Diameter and sphericity of pores that formed in the deposit

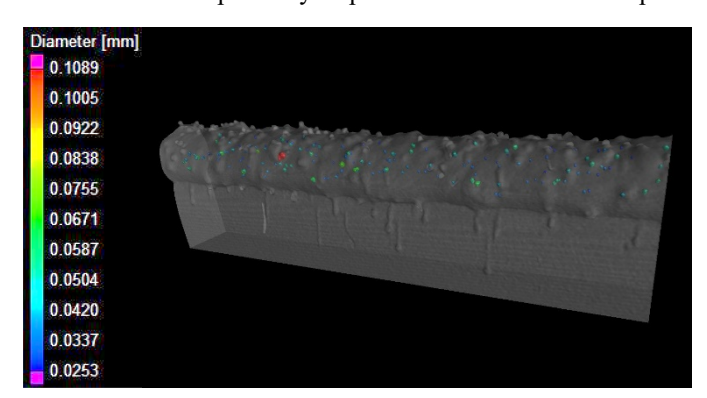


Figure 4 Representative image of single track deposit and porosity inside colored by size of diameter.

against mass flowrate were plotted in Fig. 5. Average diameter of pores decreased by $6\mu m$ whereas sphericity slightly increased by 2% with respect to increase in mass flowrate from 6g/min to 14g/min.

3.4 Microstructures analysis

Microstructures of the deposit at the surface boundary, core, and interfacial boundary between the deposit and the substrate had been inspected under the digital microscope. Representative pictures of transverse cross-section of deposit presented in Fig. 6d.

Metallurgical properties were determined by polishing and analyzing grain size/type, diffusion, and the boundary between the substrate and deposit. Columnar grain structures were found in the interfacial region between the substrate and the deposit. As power of the laser increased from 175W to 275W,

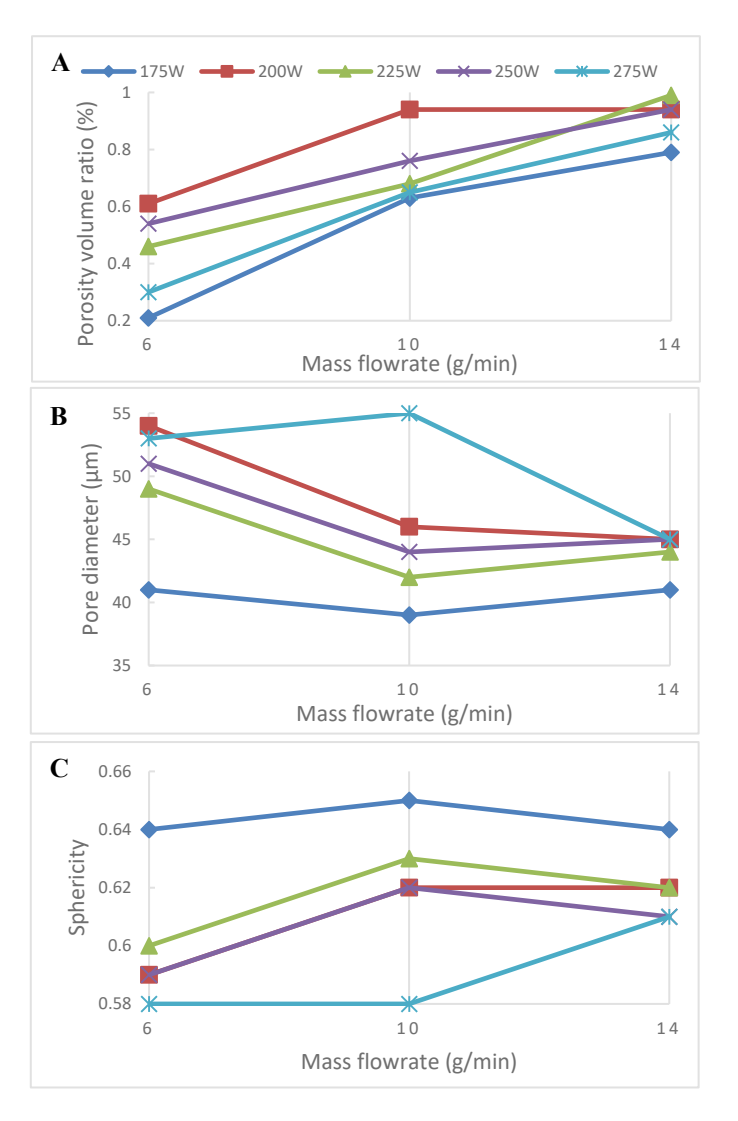


Figure 5 Porosity volume ratio (%), pore diameter (um), and sphericity of single track deposit CT scans plotted against mass flowrate. A) Porosity volume ratio vs. mass flowrate, B) pore diameter vs. mass flowrate, C) sphericity vs. mass flowrate.

the size and quantity of the columnar grains increased. At 175W (Fig. 6a), columnar grain size ranged from 10 μ m to 50 μ m. The upper range values for 225W (Fig. 6b) and 275W (Fig. 6c) were 100 μ m and 240 μ m, respectively. Range of width of columnar grains also increased from 3 to 5 μ m, 3 to 7 μ m, and 5 to 10 μ m as the power changed from 175W, 225W, and 275W, respectively.

The columnar grain structure transformed to equiaxed as it moved away from the interfacial region to the core of deposit as shown in left corner of Fig. 6e. Equiaxed grain size decreased at it moved away from the core to the surface. Average grain size of equiaxed grains in the core was $5\mu m$, and that in the surface was about $2\mu m$. Unlike grain structures in the deposit, wrought IN625 metal sheet substrate had more sharp and distinctive boundaries, and grains were more quadrilateral than round as shown in Fig. 6f.

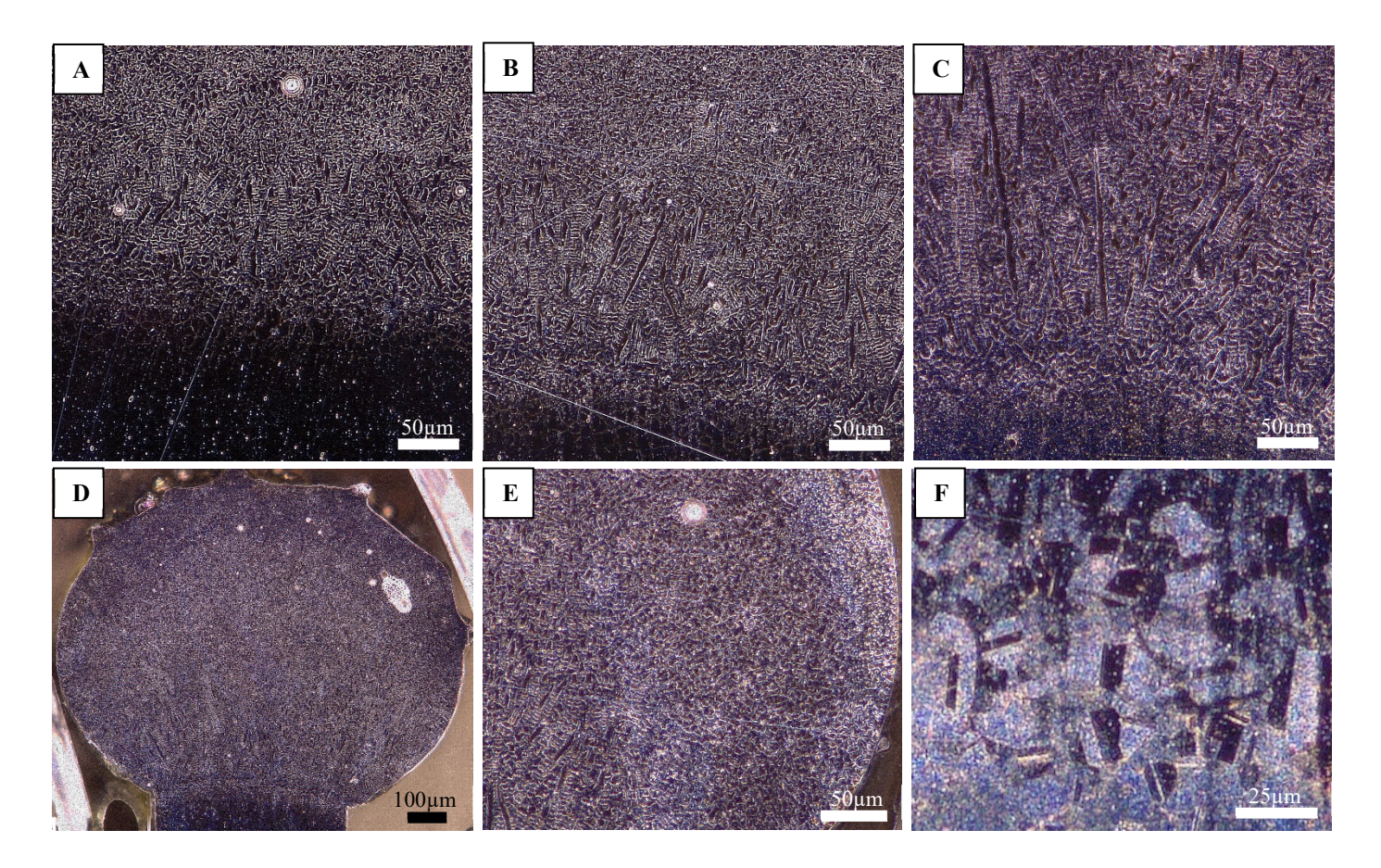


Figure 4 Representative pictures of optical microscopy with varying process parameters. A) Interfacial grain structure at 175W and 4g/min, B) 225W and 14g/min, C) 275W and 14g/min. D) Transverse cross-section of single track deposit at 250W and 14g/min. F) Evolution of grain structure from columnar (core/interfacial), large equiaxed grains (transition), to small equiaxed grains (surface). G) Grain structure of wrought IN625 metal sheet.

4. Discussion

The experiments were carried out at two extreme values of width of the substrates. Thin substrate had half of the width of the laser spot size, and thick substrate had three times of the laser spot size. With varying mass flowrate (2g/min to 20g/min) and laser power (175W to 275W), surface discoloration, geometric characteristics, porosity, and microstructures were investigated.

Surface discoloration acceptance criteria for general aerospace welding practice is that all oxidation colors are accepted except for black, or if there is a scale present according to the standard for aerospace fusion welding [31]. For discoloration of titanium, Silver, bronze, and brown colors are acceptable, and violet, blue, green, gray and white colors are not acceptable. Usually when the material goes through high temperature cycle, it appears on the surface. From the parameters that were tested in thin substrate deposition, laser power between 175W and 200W, and mass flowrate between 2g/min and 10g/min fall in acceptable rage. For thick substrate deposition, laser power between 200W and 275W, and mass flowrate equal to or greater than 16g/min were in nonacceptable range. This indicates that laser power and mass flowrate act more sensitively for thin substrate deposition and have smaller optimal window for ideal deposition.

Height of deposit increased with respect to increase in mass flowrate, but laser power did not have as much effect for both thin and thick substrate deposition. Maximum height of deposition for thick substrate deposition increased as the power increased, thin substrate deposition did not have a clear trend due to melting of the substrate. Maximum height for thick substrate deposition was 1.50mm at 275W and 20g/min, and that for thin substrate was 1.43mm at 225W and 20g/min. Linear regressions were fitted on each data set of laser power and the slope for thick substrate deposition (0.138) was slightly higher than that of thin substrate deposition (0.132).

Mass flowrate did not have much effect on the width of the substrate, but increase in power augmented the width of the deposit for both thickness. Unlike the height of the\deposition, maximum deposition width for thin substrate deposition (1.57mm) was greater at 275W and 20g/min than that for thick substrate deposition (1.22mm) at the same parameter condition. Despite the width of the thin substrate (0.5mm), enough power and mass flowrate in DED deposited more than three times width of the deposit. This could be essential for implementation in repairing thin wall features or closing existing gaps on aerospace parts. The width of the deposit was not considered in analysis when the height was below the original height of the substrate, because then the width of the bead was not due to the powder but due to the melted substrate.

Mass flowrate increased the porosity volume ratio of the deposit whereas the power did not have a clear trend in the porosity volume ratio. The standard deviation of porosity among varying power at a given mass flowrate decreased from 0.166% to 0.079% as mass flowrate increased from 6g/min to 10g/min indicating that there could be convergence in porosity with respect to change in process parameters.

The microstructure of the deposit revealed thermal effects at the interfacial region between the deposit and the substrate. Columnar grain structures in the region signifies high thermal gradient in heat transfer largely by conduction from the deposit to the substrate. As the power increased, columnar feature of the grains were more distinctively visible as more energy is put into the deposit which needs to be taken away. Size of the columnar grains increased from 50µm, 100µm to 240µm when power increased from 175W, 225W to 275W, respectively. Equiaxed grain structures were expected in the core of the deposit. Smaller equiaxed grains were present on the surface of the deposit where most of the heat was transferred by conduction. Small equiaxed grains indicates that heat was lost faster than the core. Overall the grains in the deposit were smaller and circular compared to those in the substrate.

5. Conclusion

In this study, the influences of process parameters on the discoloration of the surface, geometry of the track, porosity characteristics, and grain structure and sizes were investigated. This study particularly focuses powder DED on a substrate that has thinner width than the diameter of laser spot size, and provides a general process map to make powder-blown laser DED as effective as possible. This method is specifically relevant when a repairable part has a thin feature that need to be reconstructed with thin wall, or if starting parameters are needed to optimize the additive process. Understanding the effects of process parameters on the resultant properties will have a positive effect on the effectiveness of process optimization time and quality of the final product.

Further study on width variation of substrate between 0.5mm and 3mm with varying laser power and mass flowrate may be investigated to provide wider range of parameter optimization. Characterizing microstructure using electron backscatter diffraction (EBSD), micro-hardness test and tensile test could also widen the horizon of the effect of change in process parameters. EBSD will be used to determine in-plane crystallographic texture and how it affects mechanical properties such as stress-strain curve in tensile test, and ultimate tensile strength. All the resultant geometrical, and mechanical properties can be also tied with effective energy density of laser and effective powder deposition density to provide better understanding of powder DED on thin substrate.

Acknowledgements

The authors would like to acknowledge support from NSF CMMI-1646013, CMMI-1825640 and IIP-1631803.

References

[1] Mueller B. Additive manufacturing technologies—Rapid prototyping to direct digital manufacturing. Assembly Automation. 2012 Apr 6;32(2).

- [2 Levy GN, Schindel R, Kruth JP. Rapid manufacturing and rapid tooling with layer manufacturing (LM) technologies, state of the art and future perspectives. CIRP annals. 2003 Jan 1;52(2):589-609.
- [3] Wilson JM, Piya C, Shin YC, Zhao F, Ramani K. Remanufacturing of turbine blades by laser direct deposition with its energy and environmental impact analysis. Journal of Cleaner Production. 2014 Oct 1;80:170-8.
- [4] Kim MJ, Praniewicz M, Kurfess TR, Saldana C. Adaptive repair and digitization for hybrid manufacturing. Procedia Manufacturing. 2019 Jan 1:34:154-60.
- [5] Toyserkani E, Khajepour A, Corbin SF. Laser cladding. CRC press; 2004 Aug 12.
- [6] Lia F, Park JZ, Keist JS, Joshi S, Martukanitz RP. Thermal and microstructural analysis of laser-based directed energy deposition for Ti-6Al-4V and Inconel 625 deposits. Materials Science and Engineering: A. 2018 Feb 21;717:1-0.
- [7] Wang JF, Sun QJ, Wang H, Liu JP, Feng JC. Effect of location on microstructure and mechanical properties of additive layer manufactured Inconel 625 using gas tungsten arc welding. Materials Science and Engineering: A. 2016 Oct 31;676:395-405.
- [8] Dinda GP, Dasgupta AK, Mazumder J. Laser aided direct metal deposition of Inconel 625 superalloy: Microstructural evolution and thermal stability. Materials Science and Engineering: A. 2009 May 25;509(1-2):98-104.
- [9] Ma D, Stoica AD, Wang Z, Beese AM. Crystallographic texture in an additively manufactured nickel-base superalloy. Materials Science and Engineering: A. 2017 Jan 27;684:47-53.
- [10] Amato KN, Hernandez J, Murr LE, Martinez E, Gaytan SM, Shindo PW, Collins S. Comparison of microstructures and properties for a Ni-base superalloy (Alloy 625) fabricated by electron and laser beam melting. Journal of Materials Science Research. 2012 Apr 1;1(2):3.
- [11] Yadroitsev I, Thivillon L, Bertrand P, Smurov I. Strategy of manufacturing components with designed internal structure by selective laser melting of metallic powder. Applied Surface Science. 2007 Dec 15:254(4):980-3.
- [12] Khanzadeh M, Chowdhury S, Tschopp MA, Doude HR, Marufuzzaman M, Bian L. In-situ monitoring of melt pool images for porosity prediction in directed energy deposition processes. IISE Transactions. 2019 May 4;51(5):437-55.
- [13] Wang Z, Palmer TA, Beese AM. Effect of processing parameters on microstructure and tensile properties of austenitic stainless steel 304L made by directed energy deposition additive manufacturing. Acta Materialia. 2016 May 15:110:226-35.
- [14] Yang YG, Hass DD, Wadley HN. Porosity control in zig-zag vapordeposited films. Thin Solid Films. 2005 Jan 3;471(1-2):1-1.
- [15] Li Y, Ma J. Study on overlapping in the laser cladding process. Surface and Coatings Technology. 1997 Mar 15;90(1-2):1-5.
- [16] Pelletier JM, Sahour MC, Pilloz M, Vannes AB. Influence of processing conditions on geometrical features of laser claddings obtained by powder injection. Journal of materials science. 1993 Jan 1;28(19):5184-8.
- [17] Wu X, Zhu B, Zeng X, Hu X, Cui K. Critical state of laser cladding with powder auto-feeding. Surface and Coatings technology. 1996 Feb 1;79(1-3):200-4.
- [18] Qian M, Lim LC, Chen ZD, Chen WI. Parametric studies of laser cladding processes. Journal of Materials Processing Technology. 1997 Jan 1;63(1-3):590-3.
- [19] Costa L, Felde I, Réti T, Kálazi Z, Colaço R, Vilar R, Verő B. A simplified semi-empirical method to select the processing parameters for laser clad coatings. InMaterials Science Forum 2003 (Vol. 414, pp. 385-394). Trans Tech Publications.
- [20] Davim JP, Oliveira C, Cardoso A. Predicting the geometric form of clad in laser cladding by powder using multiple regression analysis (MRA). Materials & Design. 2008

Jan 1;29(2):554-7.

- [21] Bi G, Gasser A. Restoration of nickel-base turbine blade knife-edges with controlled laser aided additive manufacturing. Physics Procedia. 2011 Jan 1-12-402-9
- [22] El Cheikh H, Courant B, Branchu S, Hascoet JY, Guillén R. Analysis and prediction of single laser tracks geometrical characteristics in coaxial laser cladding process. Optics and Lasers in Engineering. 2012 Mar 1;50(3):413-22.
- [23] Mondal S, Bandyopadhyay A, Pal PK. Application of artificial neural network for the prediction of laser cladding process characteristics at

- Taguchi-based optimized condition. The International Journal of Advanced Manufacturing Technology. 2014 Feb 1;70(9-12):2151-8.
- [24] Saqib S, Urbanic RJ, Aggarwal K. Analysis of laser cladding bead morphology for developing additive manufacturing travel paths. Procedia Cirp. 2014 Jan 1;17:824-9.
- [25] Caiazzo F, Alfieri V. Laser-aided Directed Energy Deposition of steel powder over flat surfaces and edges. Materials. 2018;11(3):435.
- [26] Nassar AR, Keist JS, Reutzel EW, Spurgeon TJ. Intra-layer closed-loop control of build plan during directed energy additive manufacturing of Ti– 6Al–4V. Additive Manufacturing. 2015 Apr 1;6:39-52.
- [27] Nassar AR, Starr B, Reutzel EW. Process monitoring of directed-energy deposition of Inconel-718 via plume imaging. InSolid Freeform Fabrication Symposium (SFF), Austin, TX, Aug 2015 (pp. 10-12).
- [28] Seltzer D, Schiano JL, Nassar AR, Reutzel EW. Illumination and image processing for real-time control of directed energy deposition additive manufacturing. InProc Solid Freef Fab Symp 2016 (pp. 1479-1486).
- [29] Takemura S, Koike R, Kakinuma Y, Sato Y, Oda Y. Design of powder nozzle for high resource efficiency in directed energy deposition based on computational fluid dynamics simulation. The International Journal of Advanced Manufacturing Technology. 2019 Jan 1:1-5.
- [30] Sammons PM, Bristow DA, Landers RG. Height dependent laser metal deposition process modeling. Journal of Manufacturing Science and Engineering. 2013 Oct 1;135(5):054501.
- [31] AWS D17.1/D17.1M:2010-AMD1 Specification for fusion welding for aerospace applications; 2012.